Journal of Inorganic and Organometallic Polymers and Materials (2019) 29:745–757
https://doi.org/10.1007/s10904-018-1048-8

Synthesis and Optical Properties of Layered Inorganic-Imidazoline Monoliths

K. Fujii[1] · H. Hashizume[1] · S. Shimomura[1] · T. Wakahara[1] · T. Ando[1]

Received: 6 August 2018 / Accepted: 10 December 2018 / Published online: 17 December 2018

Abstract

Two types of layered inorganic-imidazoline monoliths (Mg-Imidazoline and Ni-Imidazoline) are synthesized, and optical properties (ultraviolet–visible (UV–vis) absorption and emission) arise from both inorganic and organic moieties that are covalently bonded with each other in the layered monoliths. Monoliths are synthesized under hydrothermal conditions at 170 °C and/or 150 °C using triethoxy-3-(2-imidazolin-1-yl)propylsilane (ITES) and magnesium and/or nickel acetates. X-ray diffraction (XRD) and scanning electron microscopy (SEM) analyses confirm the formation of layered compounds with interlayer distances of 1.8 nm in the Mg-Imidazoline and Ni-Imidazoline samples. Thermogravimetric and differential thermal analysis (TG-DTA) and elemental analyses show mole ratios of Mg/Si and Ni/Si and a considerable organic component. XRD and Fourier transform infrared spectroscopy (FT-IR) results show the inorganic moiety is similar to 2:1 phyllosilicates, and FT-IR spectra show several absorption peaks attributed to an imidazolyl group and Si–C. A model for Mg-Imidazoline and Ni-Imidazoline is then proposed, which has a layered structure, interlayer distance of 1.8 nm, and comprises inorganic layers with the imidazolyl group located between them. A cation (Mg^{2+} and/or Ni^{2+})-octahedral sheet is sandwiched between two siloxane sheets to form a 2:1 phyllosilicate-like layer, and each siloxane sheet bonds to the imidazolyl group via the S–C covalent bond. Mg-Imidazoline exhibits both absorption and emission in relation to the imidazolyl group, whereas Ni-Imidazoline exhibits scant emissions. The UV–Vis spectrum of Ni-Imidazoline shows absorption and weak absorption relating to the inorganic moiety and imidazolyl group, respectively.

Keywords Layered inorganic–organic hybrid · Organically functionalized phyllosilicate · Organoclay · Luminescence · Imidazoline · Ni-phyllosilicate

1 Introduction

Layered inorganic–organic hybrids have attracted much attention as potential novel materials, as the presence of both inorganic and organic moieties gives them interesting properties [1]. Many layered inorganic–organic hybrids have been prepared by intercalating organic additives into the interlayer spaces of layered inorganic materials, such as 2:1 clay minerals [2–4] and layered double hydroxides (LDHs) [5, 6], and interlayer spaces provide an attractive two-dimensional space within a solid that can be easily expanded to accommodate organic species [1–4].

The 2:1 clay minerals are part of the large phyllosilicate family [7, 8], and smectite is one of the 2:1 clay mineral groups. These minerals have layered structures in which each layer consists of an octahedral cation (such as Mg^{2+}, Al^{3+}) sheet sandwiched between two continuous two-dimensional Si tetrahedral sheets [7, 8]. Each SiO_4 tetrahedron shares

Electronic supplementary material The online version of this article (https://doi.org/10.1007/s10904-018-1048-8) contains supplementary material, which is available to authorized users.

✉ K. Fujii
FUJII.Kazuko@nims.go.jp

H. Hashizume
HASHIZUME.Hideo@nims.go.jp

S. Shimomura
SHIMOMURA.Shuichi@nims.go.jp

T. Wakahara
WAKAHARA.Takatsugu@nims.go.jp

T. Ando
ANDO.Toshihiro@nims.go.jp

[1] National Institute for Materials Science (NIMS), 1-1 Namiki, Tsukuba, Ibaraki 305-0044, Japan

three corners with neighboring tetrahedra to form a link and construct tetrahedral Si sheets. Divalent octahedral cations (such as Mg^{2+}) occupy all three sites on the octahedral sheet in trioctahedral smectites, and in dioctahedral smectites, trivalent octahedral cations (such as Al^{3+}) occupy two-thirds of total octahedral sites in dioctahedral smectites [7, 8].

There are differences in the lateral dimensions of free states between octahedral and tetrahedral sheets. The ideal dimension of a Mg trioctahedral sheet corresponds to d = 0.156 nm in the free state (which is estimated based on the lateral dimension of brucite) [7]. Similarly, the ideal dimension of an Al dioctahedral sheet corresponds to d = 0.144 nm [9], whereas the ideal dimension of a Si tetrahedral sheet is estimated at d = 0.153 ± 0.001 nm in the free state [7]. When octahedral and tetrahedral sheets are articulated into one layer, the lateral dimensions can be adjusted to eliminate this misfit [7]. The d(060) reflects the lateral dimensions and is usually employed to identify clay minerals such as smectites: it has a value of 0.153 nm for hectorite, which is one of the trioctahedral smectites [10], and a value of 0.150 nm for montmorillonite, which is a typical Al dioctahedral smectite [11].

Layered inorganic–organic monoliths with covalent bonds between the inorganic and organic moieties have also been reported [12–27]. In this study, we use the term "monolith" for this type of layered compound. Organic moieties are located within the interlayer spaces between inorganic layers within the monolith. In the 1990s, Fukushima and Tani published reports of the syntheses of layered monoliths, e.g., 2:1 type 3-(methacryloxy)propyl magnesium and nickel phyllosilicates and so on using a method known as one-pot synthesis [15, 16]. Following these reports, efforts towards synthesizing layered monoliths were also made. For example, Carrado et al. reported layered monoliths such as phenyl-hectorite [17] and Guillot et al. reported a layered monolith (a lamellar organic–inorganic nickel silicate) synthesized at 170 °C from nickel acetate and an organotrialkoxysilane, (3-aminopropyl)triethoxysilane and investigated the UV–Vis absorption and paramagnetic-ferromagnetic transition of the monolith [12]. Furthermore, Whilton et al. reported a layered monolith of organically functionalized magnesium phyllosilicate (Mg-ITES) that was synthesized at room temperature (RT) from triethoxy-3-(2-imidazolin-1-yl)propylsilane (ITES, Scheme 1) and $MgCl_2 \cdot 6H_2O$ [13].

The technique of post-grafting has also been applied to synthesize layered monoliths in cases where silanol groups are present on the surfaces of inorganic layers, such as kaolinite [18] and silicic acids [19]. Organic pendants can be grafted onto the inorganic layers by reactions between organic reagents and the surface silanol groups. However, although several layered inorganic–organic monoliths have been synthesized, the properties of the layered monoliths have not yet been fully clarified.

This present study aimed to synthesize layered inorganic–organic monoliths that exhibit optical properties. In this respect, we synthesize layered inorganic–imidazoline monoliths from ITES (Scheme 1) and two inorganic salts (magnesium acetate and nickel acetate). ITES was used as the starting organic reagent because it involves an imidazolyl group, and imidazolines have been studied in the development of novel catalysts, adsorbents [28], and inorganic/organic hybrid membranes [29]. Mg and Ni were selected as the inorganic cations. Mg-ITES was synthesized by Whilton et al. [13], but there have been no reports on UV–Vis absorption and/or the emission of layered inorganic-imidazoline monoliths. Ni-Imidazoline was selected because it is similar to Mg-Imidazoline: a six-coordinated octahedron is formed with a central Ni ion and the ionic radius of Ni^{2+} is close to that of Mg^{2+} [30]. Furthermore we analyze the UV–Vis absorption and emission of Mg-Imidazoline and Ni-Imidazoline.

Triethoxy-3-(2-imidazolin-1-yl)propylsilane (ITES)

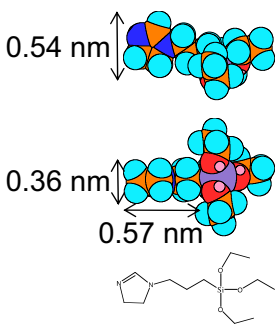

Scheme 1 Triethoxy-3-(2-imidazolin-1-yl)propylsilane (ITES)

2 Experimental

2.1 Synthesis

Mg-Imidazoline and Ni-Imidazoline were synthesized using the method reported by Guillot et al. [12] for the layered monolith, aminopropyl-nickel phyllosilicate, with some modifications. Magnesium acetate tetrahydrate ($Mg(CH_3COO)_2 \cdot 4H_2O$, 99.9%) and nickel (II) acetate tetrahydrate ($Ni(CH_3COO)_2 \cdot 4H_2O$, 99.9%) were purchased from Wako (currently: FUJIFILM Wako Pure Chemical Corporation). Each acetate was dissolved in purified water (> 18 MΩ cm) to prepare aqueous solutions of the metallic acetates. Triethoxy-3-(2-imidazolin-1-yl)propylsilane ($C_{12}H_{26}N_2O_3Si$, Aldrich, ≥ 97%, abbreviated as ITES [13], Scheme 1) was slowly added to the aqueous solutions of the metallic acetates under continuous stirring at room temperature (RT). The molar ratio of ITES to metallic acetate

Table 1 Summary of synthesis conditions

	Starting reagents		Temperatures (°C)	Times (days)
Samples				
Mg-Imidazoline	$Mg(CH_3COO)_2$	ITES	170	6
Ni-Imidazoline	$Ni(CH_3COO)_2$	ITES	150	6
References				
Mg-TEOS	$Mg(CH_3COO)_2$	TEOS	170	6
Ni-TEOS	$Ni(CH_3COO)_2$	TEOS	170	6

was 4:3 for both solutions. After sufficient stirring at RT, the starting mixtures were obtained, and these were then reacted in a Morey-type pressure vessel at 80–170 °C for 6 days [12]. The obtained crude products were washed with purified water, filtered, and then freeze-dried using a Yamato Freeze Dryer DC41 to obtain targeted samples. The sample synthesized with magnesium acetate is denoted as Mg-Imidazoline and that synthesized with nickel acetate as Ni-Imidazoline, as listed in Table 1. Other samples were synthesized with tetraethoxysilane ($Si(OC_2H_5)_4$, abbreviated as TEOS) instead of ITES, for reference, and these are denoted as Mg-TEOS and Ni-TEOS. Synthetic smectite (SWN) was purchased from the Co-op Chemical Co., Ltd (currently: Katakura & Co-op Agri Corporation).

2.2 Characterization

X-ray diffraction (XRD) measurements were conducted at RT under a dry nitrogen flow and/or air using Cu-Kα radiation (λ = 1.5405 Å) on a Rigaku RINT-2200 HF X-ray diffractometer equipped with a humidity- and temperature-controlled chamber [31]. Each powder sample was placed on an XRD specimen holder and set horizontally on the X-ray diffractometer to measure the XRD pattern of synthesized and reference samples (Mg-Imidazoline, Ni-Imidazoline, Mg-TEOS, Ni-TEOS, and SWN).

The starting mixtures and crude products were solid–liquid mixtures; therefore, samples were dropped onto quartz glass plates and then air-dried on the plates at RT. The specimen plates were then set on the X-ray diffractometer to conduct XRD measurements. Scanning electron microscopy (SEM) images were obtained using a HITACHI S-5000 at an accelerating voltage of 10 kV. Prior to SEM observations, specimens were coated with a thin layer of Pt.

Elemental analysis was conducted using an inductively coupled plasma optical emission spectrometer (ICP-OES) on Hitachi High-Tech Science Corporation SPS3520UV-DD for magnesium, silicon, and nickel. CHN analysis was conducted for carbon, hydrogen, and nitrogen, and thermogravimetric and differential thermal analysis (TG-DTA) was conducted using a Rigaku TG8101C in an Ar flow with a temperature ramp of 5°C/min to 1000 °C.

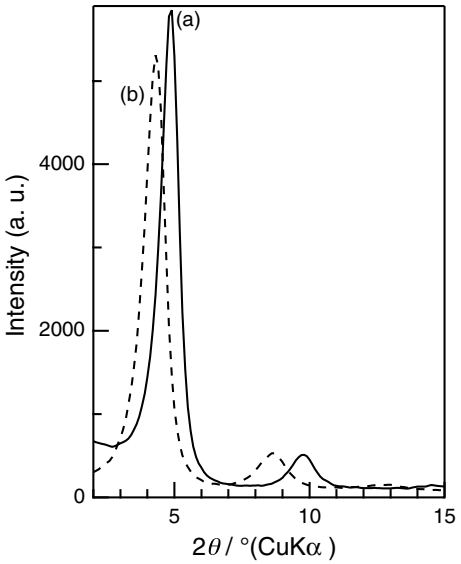

Fig. 1 XRD patterns of a sample (Mg-Imidazoline) synthesized at 170 °C for 6 days from magnesium acetate and ITES **a** acquired under N_2 flow and **b** in air

Fourier transform infrared (FT-IR) spectra were recorded on a Jasco FT/IR-4600 spectrometer. The samples were sandwiched between two KBr plates and then pressed to prepare FT-IR specimens, which were then set into the sample chamber of the FT-IR spectrometer. Dry nitrogen was passed into the specimen chamber of the FT-IR spectrometer. The recorded FT-IR spectra were corrected with software to subtract the influence of CO_2 and water vapor. Ultraviolet–visible-near-infrared (UV–Vis-NIR) spectra were measured using a Jasco V-670 UV/VIS/NIR spectrophotometer equipped with an integrating sphere, and emission spectra were observed using a Hitachi F-7000 fluorescence spectrophotometer.

3 Results

3.1 XRD

A strong XRD peak was observed at a low angle (d = 1.8 nm) from the synthesized sample of Mg-Imidazoline (Fig. 1a); this XRD pattern was measured under a controlled relative humidity of 5% in a nitrogen flow. Other peaks in this region are attributed to higher order reflections of this strong diffraction peak, and these peaks shifted when the XRD pattern was measured under air (Fig. 1b). The measured XRD peak position corresponds to a d value of 2.0 nm (Fig. 1b).

It is well known that changes in humidity can cause a shift in XRD peaks of hydrophilic smectites. H_2O molecules are

intercalated into the interlayer spaces of the smectites from the atmosphere and the interlayer distances of smectites are expanded under an atmosphere with moderate to high humidity [8, 32]. When environmental humidity decreases, these H_2O molecules are deintercalated from the interlayer spaces. Therefore, the interlayer distances of the smectites change with changes in humidity. In this respect, the H_2O molecules were intercalated into the interlayer spaces of the synthesized samples when exposed to the atmosphere. Hereinafter, we show XRD patterns measured under a nitrogen flow and with a relative humidity controlled to be lower than 6%.

Three XRD peaks were observed in the low-angle range for Mg-Imidazoline synthesized at 170 °C for 6 days (Fig. 2a) and Ni-Imidazoline synthesized at 150 °C for 6 days (Fig. 2b). Reflection peaks intensified (Fig. 3) and IR absorption, which is attributed to Si–O–Si, grew at approximately 1000 cm^{-1} (Fig. 4) as synthesis temperatures increased. However, the XRD pattern (Fig. 3a) exhibited reflection peaks attributed to nickel (d = 0.204 and 0.176 nm) for the sample synthesized at 170 °C from a starting mixture consisting of ITES and nickel acetate. We refer to the sample synthesized at 150 °C for 6 days from ITES and nickel acetate as Ni-Imidazoline, whereas the other sample (Mg-Imidazoline) and reference samples were synthesized at 170 °C, as listed in Table 1.

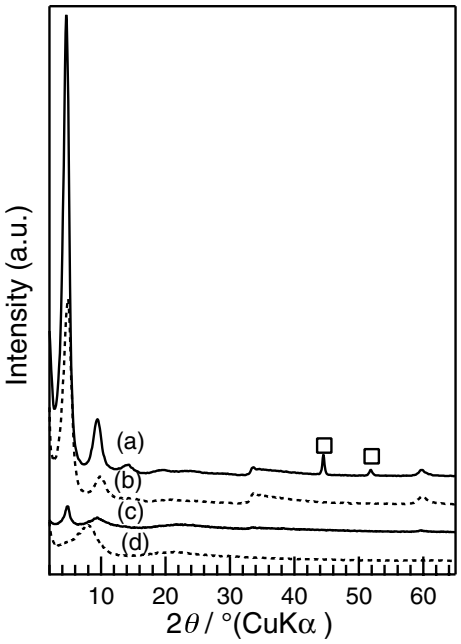

Fig. 3 XRD patterns of samples synthesized at **a** 170 °C, **b** 150 °C (Ni-Imidazoline), and **c** 80 °C for 6 days using nickel acetate and ITES, and **d** starting mixture for Ni-Imidazoline, all recorded under N_2 flow. The diffraction peaks assigned to nickel are marked (square box). The patterns were shifted vertically without any enlargement. Pattern **b** is the same as that in Fig. 2b

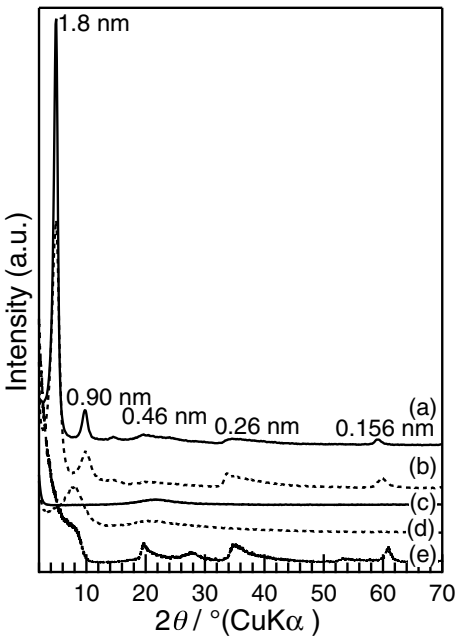

Fig. 2 XRD patterns of **a** Mg-Imidazoline, **b** Ni-Imidazoline, starting mixtures for **c** Mg-Imidazoline and **d** Ni-Imidazoline, and **e** the synthetic smectite (SWN) all recorded under N_2 flow. The patterns were shifted vertically without any enlargement. Pattern **a** is the same as that in Fig. 1a

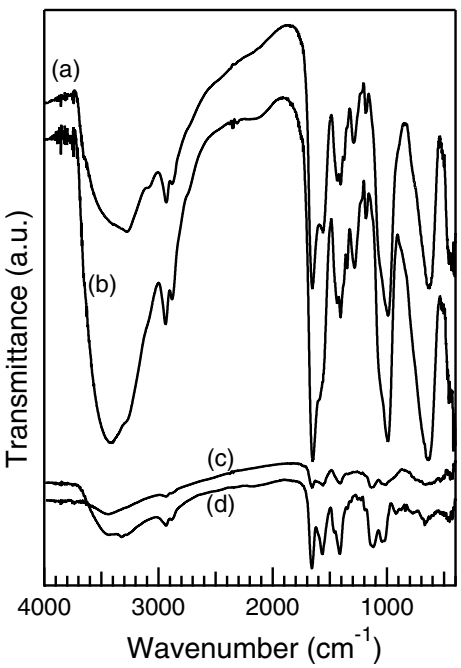

Fig. 4 FT-IR spectra of samples synthesized at **a** 170 °C, **b** 150 °C (Ni-Imidazoline), and **c** 80 °C for 6 days using nickel acetate and ITES, and **d** starting mixture for Ni-Imidazoline. Spectra were shifted vertically without any enlargement

The most intense reflection peak in the XRD patterns corresponds to a d value of 1.8 nm (Fig. 2a, b). Other peaks in the low angle range are due to higher order reflections of the most intense reflections. The XRD patterns also show asymmetric peaks corresponding to d values of 0.26 and 0.46 nm in Mg-Imidazoline (Fig. 2a) and d values of 0.27 and 0.45 nm in Ni-Imidazoline (Fig. 2b). In addition, reflection peaks are observed at 2θ values of around 60° (Fig. 2a, b), and corresponding d values are 0.156 (Fig. 2a) and 0.155 nm (Fig. 2b) for Mg- and Ni-Imidazoline, respectively. These reflection peaks were not observed in the starting mixtures (Fig. 2c, d), and none of the XRD peaks in the XRD patterns of Mg-Imidazoline and Ni-Imidazoline are attributed to the starting reagents or any by-product (Fig. 2a, b).

The XRD patterns of Mg-Imidazoline and Ni-Imidazoline (Fig. 2a, b) are thus similar to that of synthetic smectite (SWN) (Fig. 2e), in which asymmetric peaks are indexed as (130), (200) (d ≈ 0.26 nm) and (020), (110) (d ≈ 0.45 nm), the reflection peak corresponding to a d value of 0.152 nm is indexed to the (060), (330) planes, and the d value associated with a reflection peak in the low angle range corresponds to the interlayer distance (Fig. 2e) [7].

XRD analysis showed only a halo pattern around a 2θ of 20° for the starting mixture of Mg-Imidazoline (Fig. 2c), and it is well known that halo patterns are observed around this region in relation to scattering by an amorphous phase. Another broad diffraction (d of 1.1 nm) was observed in the starting mixture for Ni-Imidazoline (Fig. 2d), and we speculate that this broad diffraction (d ≈ 1.1 nm) is attributed to the self-assembly aggregation of ITES. Ni^{2+} ions would play a certain role in the assembly.

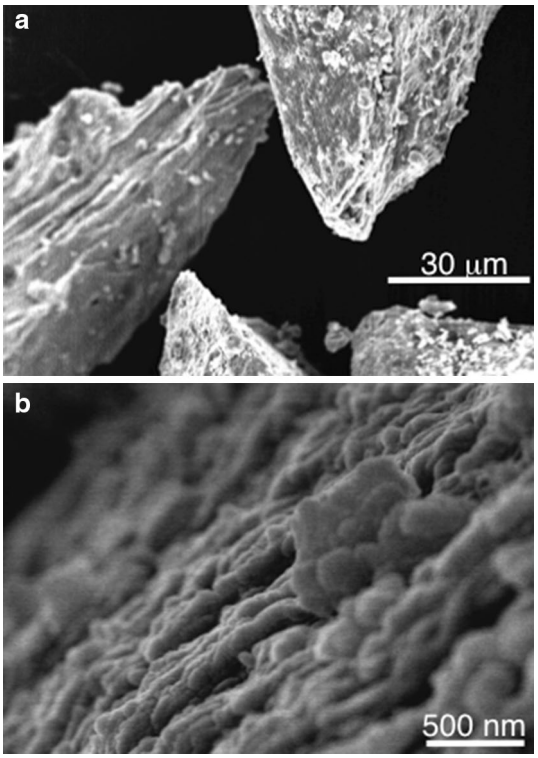

Fig. 5 **a** SEM and **b** magnified SEM images of Mg-Imidazoline

3.2 SEM Image

The SEM image shows layered morphologies that are beyond several µm (Fig. 5a), and a magnified SEM image shows the layer consists of aggregated small particles with sizes of approximately 200 nm (Fig. 5b). These small particles are stacked in the order of the stacking direction, which results in a layered assembly. However, SEM observations did not provide any information relating to the order in a lateral direction.

3.3 Elemental Analyses and TG-DTA

The ICP-OES analysis yielded contents for Si and Mg and/or Ni in Mg-Imidazoline and/or Ni-Imidazoline as listed in Table 2, and CHN analysis demonstrated results for C, H, and N within the samples (Table 2).

Figure 6 shows the TG-DTA curves in an Ar flow for Ni-Imidazoline (Fig. 6a, b) and reference samples, Ni-TEOS (Fig. 6c, d) and synthetic smectite SWN (Fig. 6e, f). The DTA curve for Ni-Imidazoline (Fig. 6b) demonstrates an endothermic event starting at RT with a peak at around 63 °C, which is accompanied by a weight loss of 11.8% from RT to 95 °C and of 13.4% from RT to 202 °C for Ni-Imidazoline (Fig. 6a). It is well known that the TG curves of smectites indicate weight loss (as shown in Fig. 6e, f) due

Table 2 Results of the elemental analyses

Samples	Results (%)					
	Si	Mg	Ni	C	H	N
Samples						
Mg-Imidazoline	8.7	8.4		22.87	5.18	6.94
Ni-Imidazoline	5.9		32.1	14.89	3.82	4.51
References						
Mg-TEOS	34.5	3.4				
Ni-TEOS	18.1		33			

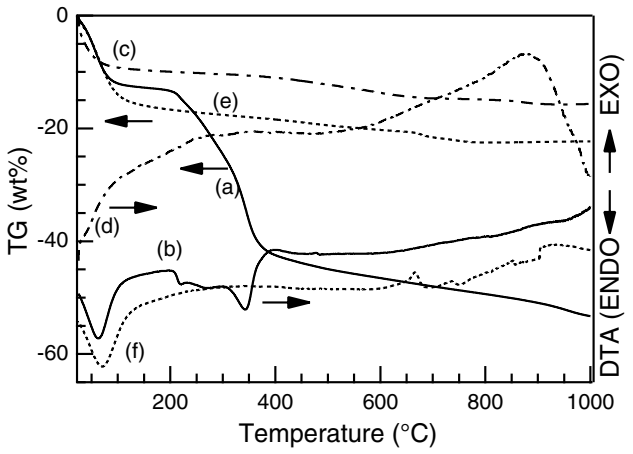

Fig. 6 TG-DTA curves in an Ar flow for **a** and **b** Ni-Imidazoline and reference samples, **c** and **d** Ni-TEOS and **e** and **f** the synthetic smectite (SWN)

to the desorption of interlayer water and water adsorbed on the external surfaces of SWN [33]. The TG-DTA curves show that Ni-Imidazoline underwent a drastic weight loss of 28.1% during several endothermic events from 202 to 382 °C (Fig. 6a, b). The TG curve of Ni-Imidazoline shows a prolonged weight loss of 11.7% up to 1000 °C (Fig. 6a), and weight loss caused by dehydration from lattices of smectites has been reported at around 700 °C [34, 35]. The final residual weight was 46.7% for Ni-Imidazoline (Fig. 6a), and the color of the sample turned from an original color of pale green to black after the TG-DTA measurement. However, the TG curves of reference samples do not indicate this drastic weight loss [Ni-TEOS (Fig. 6c) and SWN (Fig. 6e)]. The differences between these TG results suggest that the drastic weight loss is caused by the decomposition of the organic component in Ni-Imidazoline.

Similarly, the TG-DTA curves of Mg-Imidazoline (not shown) showed a weight loss of 13.4% accompanying an endothermic event from RT to 202 °C, and a drastic weight loss of 35.3% from 202 to 503 °C (not shown). Furthermore, weight losses of 10.1% for Ni-TEOS (Fig. 6c), 8.1% for Mg-TEOS (not shown) and 16.7% for SWN (Fig. 6e) were observed from RT to around 200 °C.

3.4 FT-IR Spectroscopy

Figure 7 shows FT-IR spectra of Mg-Imidazoline (spectrum a) and Ni-Imidazoline (spectrum b). Spectra c–e show results for reference samples as follows: (c) Mg-TEOS, (d) Ni-TEOS, and (e) ITES. Strong and broad IR absorption peaks were observed at around 1000 cm^{-1} for the synthesized samples (Mg-Imidazoline and Ni-Imidazoline) and reference samples (Mg- and Ni-TEOS), and these absorption peaks are attributed to the Si–O–Si stretching vibrations.

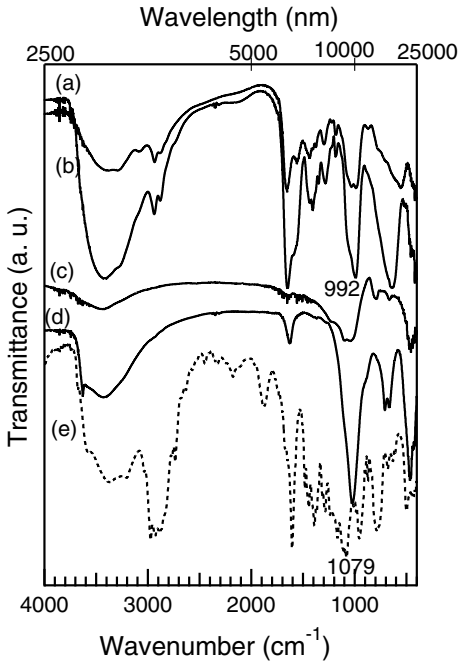

Fig. 7 FT-IR spectra of **a** Mg-Imidazoline, **b** Ni-Imidazoline, **c** Mg-TEOS, **d** Ni-TEOS, and **e** ITES. Spectra were shifted vertically without any enlargement, except for the spectrum **e** which was reduced by a factor of 1/2. Spectrum **b** is the same as that in Fig. 4b

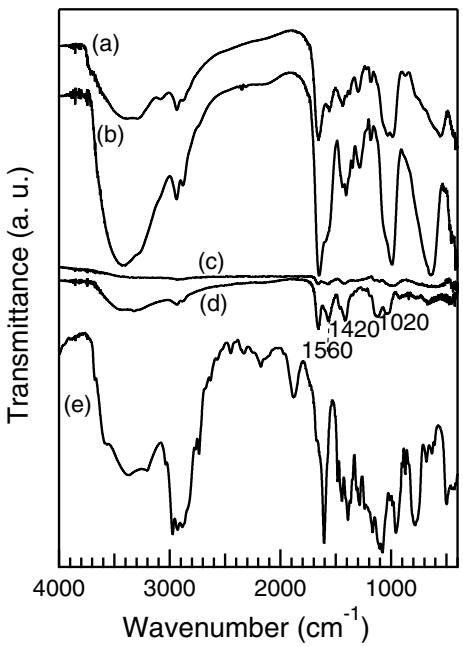

Fig. 8 FT-IR spectra of **a** Mg-Imidazoline, **b** Ni-Imidazoline, starting mixtures for **c** Mg-Imidazoline and **d** Ni-Imidazoline, and **e** ITES. Spectra were shifted vertically. Spectrum **c** was enlarged by a factor of 2. Spectrum **e** was reduced by a factor of 1/2. Spectra **a, b**, and **e** are the same as those in Fig. 7a, b, e, respectively

Such peaks have also been observed around this wavenumber region for 2:1 phyllosilicates [9] and previously reported monoliths such as organically modified 2:1 phyllosilicates [12, 13, 15, 17]. An absorption band at 1079 cm^{-1} was observed for ITES (Fig. 7e) and was assigned to Si–O–C [36].

A broad IR absorption band was observed at around 1020 cm^{-1} for the starting mixture of Ni-Imidazoline (Fig. 8d), and another broad IR absorption band was observed at around 990 cm^{-1} for Mg-Imidazoline, Ni-Imidazoline, and the starting mixture of Mg-Imidazoline (Fig. 8a–c).

An IR absorption peak was observed at 3630 cm^{-1} in the reference sample, Ni-TEOS (Fig. 7d). This peak is assigned to an O–H stretching mode for the OH group in the Ni trioctahedral sheet in the inorganic moiety. It is well known that characteristic absorptions are observed for the O–H stretching mode in 2:1 phyllosilicates in a region from 3610 to 3640 cm^{-1} [9]. Absorption has been reported in this region for the O–H groups in the organically modified 2:1 phyllosilicates [12, 17].

Broad absorption bands at around 3400 cm^{-1} and absorption peaks at around 1650 cm^{-1} are attributed to adsorbed water for Mg- and Ni-Imidazoline and Mg- and Ni-TEOS (Fig. 7a–d) [15, 17]. The XRD results show that H_2O molecules are intercalated into the interlayer space of the synthesized samples, as described above, and demonstrate that H_2O molecules are deintercalated from the interlayer space under a nitrogen flow and at a relative humidity lower than 6%. The powder samples were directly exposed under the nitrogen flow for the XRD measurements, as they were not covered in the XRD sample holder, and they were sandwiched between the two KBr plates and pressed in preparation for FT-IR measurements. Therefore, dehydration might be more difficult for the FT-IR specimen than for the XRD specimen.

The IR spectra show IR absorption peaks related to cation octahedral sheets at low wavenumber regions for the synthesized and reference samples (Fig. 7a–d). An absorption peak is observed at around 557 cm^{-1} in Mg-Imidazoline (Fig. 7a), which is attributed to Mg–O vibration. Some reports have assigned absorption at around 535 cm^{-1} to the Mg–O vibration of the Mg-trioctahedral sheet in talc [37] and the Mg octahedral sheet in 2:1 type 3-(methacryloxy) propyl magnesium phyllosilicate [15, 21, 22]. Absorption at around 640 cm^{-1} (Fig. 7b) can be attributed to Ni–O vibration of the Ni octahedral sheet in Ni-Imidazoline [9], and absorption at around 666 cm^{-1} (Fig. 7c) is attributed to the Mg–O vibration in the Mg-trioctahedral sheet of Mg-TEOS [9]. Furthermore, an absorption peak at around 791 cm^{-1} can be attributed to OH groups bound to the Mg^{2+} ions of Mg-TEOS (Fig. 7c). The FT-IR spectrum show two relatively sharp peaks at 668 and 709 cm^{-1} for Ni-TEOS (Fig. 7d): the former peak is attributed to the Ni–O vibration in the Ni-trioctahedral sheet [9], and the latter is attributed to the hydroxyl groups bound to Ni^{2+} ions in the Ni-trioctahedral sheet [9]. The FT-IR spectra also show broad trailing absorption on the higher wavenumber sides of the absorption peaks at around 557 cm^{-1} for Mg-Imidazoline (Fig. 7a) and 641 cm^{-1} for Ni-Imidazoline (Fig. 7b). One possible explanation for this is that several absorption peaks attributed to the OH groups would result in broad, trailing absorption at higher wavenumbers.

The FT-IR spectra show several peaks at around 2900 cm^{-1} in Mg-Imidazoline, Ni-Imidazoline, and ITES (Fig. 7a, b, e), but not in the reference samples (Fig. 7c, d). The absorptions at around 2936 and 2880 cm^{-1} are assigned to antisymmetric and symmetric CH_2 vibrations (Fig. 7a, b, e) [12, 15, 22, 37]. The absorption at 2974 cm^{-1} is assigned to C-H vibrations of the CH_3 group (Fig. 7e), and this is not observed in Mg-Imidazoline and Ni-Imidazoline (Fig. 7a, b). The FT-IR spectra further show many absorption peaks in a region from 1100 to 1600 cm^{-1} in Mg-Imidazoline, Ni-Imidazoline, and ITES (Fig. 7a, b, e), but these peaks are not apparent in the reference sample spectra (Fig. 7c, d). These absorptions are attributed to characteristic absorptions of an imidazolylsilyl group, e.g., C = N (1605 cm^{-1}), CH_2 (1440 cm^{-1}), C-N (1284 cm^{-1}), and Si-C (1186 cm^{-1}) [12, 13, 20, 22]. Absorption peaks at 1390 (C–CH_3), 1239 (C–O), and 1079 cm^{-1} (Si–O–C) are only observed for ITES (Fig. 7e) [15].

Thus, the FT-IR spectra indicate absorption due to the imidazolylsilyl group in Mg-Imidazoline, Ni-Imidazoline, and ITES (Fig. 7a, b, e), and absorption peaks relating to the alkoxyl group are not present in the Mg-Imidazoline and Ni-Imidazoline spectra. Absorption peaks are observed at 1420 and 1560 cm^{-1} in the FT-IR spectra of starting mixtures (Fig. 8) and crude products of Mg-Imidazoline and Ni-Imidazoline, and these are assigned to COO^- symmetric and antisymmetric stretching vibrations [12].

3.5 UV–Vis-NIR Spectroscopy

Figure 9 shows UV–vis spectra for samples and ITES as the reference; reflectance is shown on the vertical axis and wavelength on the horizontal axis. Absorption at around 335 nm is attributed to the imidazolyl group, and this absorption is weaker for Ni-Imidazoline (Fig. 9b) than for Mg-Imidazoline and ITES (Fig. 9a, c). Absorption peaks at around 390 nm (25,641 cm^{-1}) and 680 nm (14,706 cm^{-1}) are observed for both Ni-Imidazoline and reference Ni-TEOS (Fig. 10a, b), and shoulders of these absorption peaks are also observed at a longer wavelength (Fig. 10a, b).

The NIR spectrum show broad absorption at around 8660 cm^{-1} (1150 nm) for Ni-TEOS (Fig. 11d), which is attributed to the transition $^3A_{2g} \rightarrow {}^3T_{2g}$ of Ni (II) [38, 39].

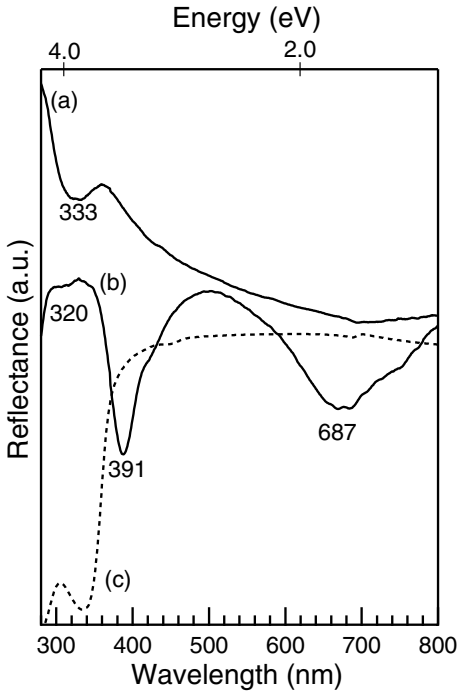

Fig. 9 UV–Vis spectra of **a** Mg-Imidazoline, **b** Ni-Imidazoline, and **c** ITES. Spectra were shifted vertically. Spectrum **c** was reduced by a factor of 1/20

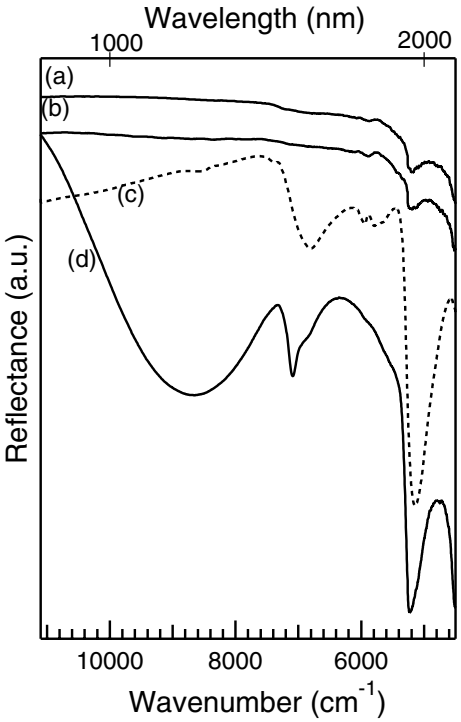

Fig. 11 Near-infrared (NIR) spectra of **a** Mg-Imidazoline, **b** Ni-Imidazoline, **c** Mg-TEOS, and **d** Ni-TEOS. Spectra were shifted vertically without any enlargement

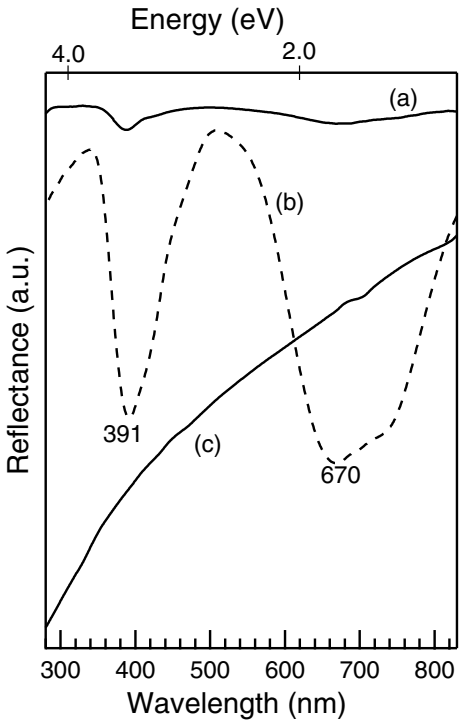

Fig. 10 UV–Vis spectra of **a** Ni-Imidazoline, **b** Ni-TEOS, and **c** Mg-TEOS. Spectra were shifted vertically. Spectrum **a** is the same as that in Fig. 9b

Absorption is observed at around 7092 cm^{-1} (1410 nm) for Ni-TEOS (Fig. 11d), and this is ascribed to an overtone of absorption due to the O–H stretching mode observed in the FT-IR spectrum (Fig. 7d). An absorption peak is observed at around 6812 cm^{-1} (1468 nm) for Mg-TEOS (Fig. 11c), and a shoulder is observed at 6810 cm^{-1} for Ni-TEOS (Fig. 11d); these absorptions are attributed to the overtone of the absorption due to adsorbed water (Fig. 7c, d). Absorptions are observed at around 5200 cm^{-1} (1925 nm) for Mg- and Ni-Imidazoline and Mg- and Ni-TEOS (Fig. 11a–d); these are ascribed to combination bands of the absorptions attributed to adsorbed water (Fig. 7a–d).

3.6 Emission

Emission is observed at around 410 nm for Mg-Imidazoline and ITES (Fig. 12a, c) and is attributed to the imidazolyl group. This emission was not observed for Ni-Imidazoline (Fig. 12b) [the excitation wavelength was set at 320 nm where absorption was observed for Ni-Imidazoline (Fig. 9b)]. Furthermore, emission was observed for Mg-Imidazoline and ITES but not observed for Ni-Imidazoline when samples were excited at 335 and 380 nm (not shown); these wavelengths are peak positions of the UV–Vis spectra for Mg-Imidazoline and ITES (Fig. 9a, c) and Ni-Imidazoline (Fig. 9b).

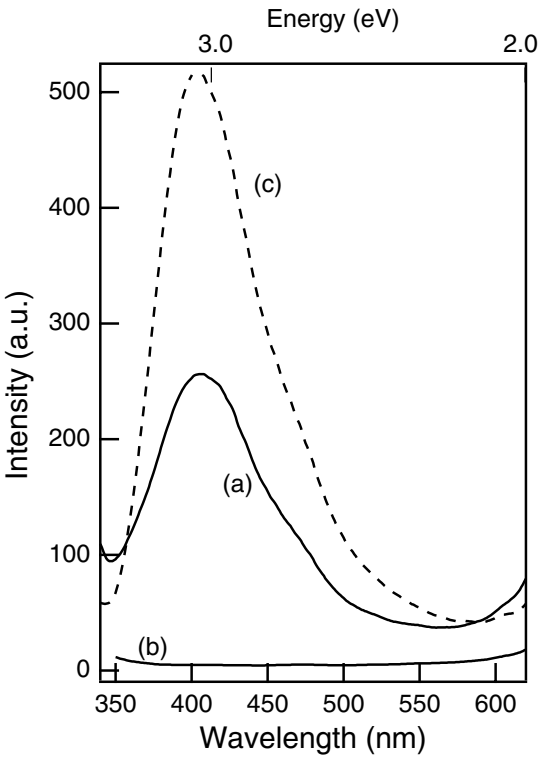

Fig. 12 Emission spectra of **a** Mg-Imidazoline, **b** Ni-Imidazoline, and **c** ITES. The excitation wavelength was set at 320 nm

4 Discussion

4.1 Structure Models of Mg-Imidazoline and Ni-Imidazoline

For the Mg- and Ni-Imidazoline samples, XRD (Fig. 2a, b) and SEM (Fig. 5) analyses demonstrate synthesis of layered compounds with an interlayer distance of 1.8 nm, and XRD patterns (Fig. 2a, b) for these two samples show intense reflection peaks in the low angle range, asymmetric peaks, and reflection peaks at 2θ of around 60°, which are similar to those of synthetic smectite (SWN) (Fig. 2e). It is suggested, in a similar manner to previously reported investigations [12, 13, 15, 17, 21, 22], that Mg-Imidazoline and Ni-Imidazoline are layered compounds similar to smectites.

The FT-IR spectra indicate absorptions attributed to Si–O–Si networks (at around 1000 cm^{-1}) and Mg and/or Ni octahedral sheets in the synthesized and reference samples (Fig. 7). The IR absorption peaks relating to the octahedral sheets shifted depending on the sample's components. These results suggest for Mg-Imidazoline and Ni-Imidazoline that the inorganic moiety consists of Mg- and/or Ni-octahedral sheets and siloxane sheets. The results of FT-IR are consistent with those of XRD and SEM, which suggest that Mg- and Ni-Imidazoline are similar to smectite.

The absorption peak related to the octahedral cation sheet was sharper for Ni-TEOS (Fig. 7d) than for the other samples (in the low wavenumber region in Fig. 7a–c). This result is consistent that for absorption assigned to O–H stretching mode at 3630 cm^{-1}, which is observed only for Ni-TEOS. These differences in FT-IR spectra suggest that the structure of the Ni-trioctahedral sheets of Ni-TEOS has higher regularity than that of the octahedral sheets of Mg- and Ni-Imidazoline and Mg-TEOS.

Elemental (Table 2) and TG-DTA (Fig. 6) analyses demonstrate a considerable organic component for Mg- and Ni-Imidazoline. The weight contents for each element (Table 2) correspond to molar ratio of 3.5:3.9:21.5:58.0:5.6 for Si:Mg:C:H:N, for Mg-Imidazoline; corresponding molar ratio for Ni-Imidazoline is similar at 2.4:6.2:14.2:43.2:3.7 for Si:Ni:C:H:N; and that of C/Si for Mg-Imidazoline and Ni-Imidazoline are 6.1 and 5.9, respectively. The imidazolylsilyl group, 3-(2-imidazolin-1-yl)propylsilyl group ($C_6H_{11}N_2Si$) involves six carbon and one-silicon atoms. The FT-IR spectra indicate absorption due to the imidazolylsilyl group, i.e., at around 2900 (CH_2), 1605 (C=N), 1440 (CH_2), 1284 (C–N) and 1186 cm^{-1} (Si–C) for Mg-Imidazoline and Ni-Imidazoline (Fig. 7a, b); these results indicate that Mg- and Ni-Imidazoline involve the imidazolylsilyl group.

The FT-IR spectra indicate absorption due to the alkoxyl group for ITES but not for Mg-Imidazoline and Ni-Imidazoline. These results suggest that ITES is hydrolyzed and it then reacts with metal acetates and with itself to form the Si–O–Si network in the monoliths under stirring when starting mixtures are prepared and under subsequent hydrothermal conditions. In an ideal smectite structure, silicon tetrahedra are linked with neighboring tetrahedra by sharing three corners to form the Si tetrahedral sheet with a hexagonal mesh pattern [7]. It should be difficult for Mg-Imidazoline and Ni-Imidazoline to form a perfect Si tetrahedral sheet because each Si needs to bond to one C of the imidazolyl group. Instead, each $RSiO_3$ unit bonds to two neighboring $RSiO_3$ units via Si–O–Si bonds to form a continuous two-dimensional organosiloxane network in Mg-Imidazoline and Ni-Imidazoline. Here R denotes the imidazolyl group, 3-(2-imidazolin-1-yl)propyl group ($C_6H_{11}N_2$).

The analytical results of XRD, SEM, TG-DTA, elemental analyses, FT-IR, and UV–Vis-NIR enabled a model structure to be proposed, which is shown as Scheme 2a and b for Mg-Imidazoline and Ni-Imidazoline. A molar ratio for Si:M (Mg and/or Ni) of 4:3 was expected for the model structure (Scheme 2a, b) with a inorganic layer analogous to the layer of the 2:1 phyllosilicates. A chemical composition is described as

$$\left(Li^{+}_{x}nH_2O\right)\left(Mg_{3-x}Li_x\right)Si_4O_{10}(OH)_2 \quad (1)$$

for a typical reported hectorite [33].

However, the structure model illustrated in Scheme 2b would be difficult because of the steric hindrance of the imidazolyl group, and elemental analyses indicated that the molar ratios of M/Si are 1.1 and 2.6 for Mg-Imidazoline and Ni-Imidazoline, which is much larger than the expected value (0.75) for the model (Scheme 2b). The results of XRD, TG-DTA, and FT-IR demonstrate that H_2O molecules are included in the Mg-Imidazoline, Ni-Imidazoline, and reference samples (Mg- and Ni-TEOS). Therefore, these results would lead to a proposed model that has interlayer water, interlayer exchangeable cations, and further defects in the Si site in the tetrahedral sheets that balance the charge with the interlayer cations. Assuming this model, a composition can be expressed as

$$\left(Ni^{2+}_{0.34}5H_2O\right)Ni_3Si_{3.8}O_{10}(OH)_2 \quad (2)$$

for the reference sample, Ni-TEOS. We assume for calculation of a ratio of water that interlayer water causes all the weight loss detected from RT to around 200 °C by TG-DTA (Fig. 6c). A layer charge of 0.68 is calculated for the formula, which is comparable with those (from about 0.2 to 0.6) reported for smectites [40].

We similarly attempted to calculate tentative compositions as

$$\left(Ni^{2+}_{3.2}8.2H_2O\right)Ni_3R_{2.4}Si_{2.4}O_p(OH)_q \quad (3)$$

and

$$\left(Mg^{2+}_{0.94}9.5H_2O\right)Mg_3R_{3.5}Si_{3.5}O_p(OH)_q \quad (4)$$

for Ni-Imidazoline and Mg-Imidazoline, respectively. Scheme 2c and d illustrate tentative structure models for layers corresponding to the above tentative compositions for Ni-Imidazoline (Scheme 2c) and Mg-Imidazoline (Scheme 2d), respectively.

Compositions with such large defects in imperfect Si tetrahedral sheets have been previously proposed for layered inorganic–organic monoliths [12, 21]. These defects are not only formed to balance the charge of the interlayer exchangeable cations but also for the steric hindrance of the imidazolyl group. $RSiO_3$ units can be linked to form a continuous two-dimensional organosiloxane in Mg-Imidazoline with the chemical formula (4) as in a previously reported monolith (APS-H), where alkylammonium and Mg-phyllosilicate-like moieties bond covalently with each other. The chemical composition is $\left(Li_{0.017}\right)R'_{0.43}Mg_3Si_{3.22}O_p(OH)_q$ [22], where R′ is dimethyl(octadecyl)propyl ammonium group, $C_{18}H_{37}N^+(CH_3)_2C_3H_6$.

The density of the Si atom is very poor in the model structure illustrated in Scheme 2c, and with the chemical formula (3), each Si atom would be located too far from its nearest neighboring Si atom. Therefore, the Si–O–Si network would be hardly formed in the model (Scheme 2c).

The large molar ratio of 2.6 for Ni/Si in Ni-Imidazoline suggested another model with a Ni metal nanoparticle within the interlayer space, and the composition calculated as

$$\left(Ni^{NP}_{1.5}Ni^{2+}_{0.94}nH_2O\right)R_{3.5}Si_{3.5}Ni_3O_p(OH)_q \quad (5)$$

where Ni^{Np} is one Ni atom in the Ni metal nanoparticle.

The formation of metal nanoparticles within the interlayer space of clays has previously been reported [41, 42]. We observed XRD peaks attributed to Ni metal for the sample synthesized at 170 °C from the starting mixture consisting of ITES and nickel acetate (Fig. 3a). As the synthesis temperature was lower (150 °C) for Ni-Imidazoline than that for the sample (170 °C), it was considered that the Ni metal would be smaller in Ni-Imidazoline than in the sample synthesized at 170 °C, which would cause a lack of any reflection peak attributed to the Ni nanoparticle in the XRD pattern for Ni-Imidazoline (Fig. 2b). A lack of XRD peaks for systems including metal nanoparticles has previously been reported [41], although XRD peaks for another system with cubic Cu metal larger than the nanoparticles have been reported [42].

The d (060) reflects the lateral dimensions and is therefore usually employed in the identification of smectites, as previously described in "Introduction". The measured d value for Mg-Imidazoline (Fig. 2a) was 0.156 nm, which is consistent with the lateral dimension of the Mg trioctahedral sheet in the free state. $RSiO_3$ units form continuous organosiloxane sheets instead of the perfect Si tetrahedral sheet in Mg-Imidazoline and Ni-Imidazoline. Consequently, the lateral dimensions are dominated by Mg- and Ni-octahedral sheets in the inorganic layers of Mg-Imidazoline and Ni-Imidazoline. Such d values, which are larger than those of trioctahedral smectites, have been observed in previously reported layered inorganic–organic monoliths [12, 13, 15], in which 2:1 type phyllosilicate-like structures consisting of octahedral sheets and imperfect –C–SiO_3 tetrahedral sheets are linked by organic side chains through an –Si–C– covalent bond [12, 13, 15].

The d value of 0.155 nm measured for Ni-Imidazoline was less than that measured for Mg-Imidazoline (0.156 nm). Indeed, we cannot discuss such a small difference as a significant difference in the results based on the XRD measurements. Previous reports have also shown a tendency for the d value to be shorter for the monolith with Ni as the octahedral cation than that for the monolith with Mg as the octahedral cation [12, 15]. In addition, it is well known that the d value of nickel hydroxide is less than that of brucite (magnesium hydroxide) [43].

To summarize, we ultimately propose a model structure corresponding to the composition formulae (4)

(Mg-Imidazoline) and (5) (Ni-Imidazoline), which are depicted in Scheme 2a and d. The Mg- and/or Ni-octahedral sheet is sandwiched between the two imidazolylsiloxane sheets in the layer of the monoliths, as shown in Scheme 2d. $RSiO_3$ units are linked to the neighboring Mg- and/or Ni-octahedral sheets, and the $RSiO_3$ units simultaneously form the Si–O—Si network of the imidazolylsiloxane sheets. The imidazolyl group (3-(2-imidazolin-1-yl)propyl group) is located between the 2:1 phyllosilicate-like layers and bonds to them through Si-C covalent bonds. Therefore, the proposed model is that of an imidazolyl derivative of a 2:1 phyllosilicate.

The exchangeable cations (Mg^{2+} and/or Ni^{2+}), H_2O molecules, and organic moiety are immobilized within the interlayer space of the proposed model (Scheme 2a and d). The Ni metal nanoparticle is also located between the interlayer space of the proposed model in the case of Ni-Imidazoline. As the interlayer exchangeable cations (Mg^{2+} and Ni^{2+}) are hydrated by H_2O molecules, $[Ni(H_2O)_6]^{2+}$ is formed between the interlayer space. The interlayer distance is 1.8 nm, and we can thus estimate a Δd value of 0.85 nm by assuming that the thickness of the inorganic moiety is the same as the 0.95 nm thickness of the 2:1 layer of smectites [44]. Various models can be proposed for the arrangements of the organic moiety within such a relatively large interlayer space, and we illustrate one such model arrangement in Scheme 2a.

4.2 Species Facilitating Reactions During Synthesis

The results of FT-IR (Fig. 7) suggest that the alkoxysilyl group of ITES reacted to form Si–O–Si. No acid or base reagents were added to the reaction media, as is common when facilitating hydrolysis and condensation reactions of alkoxides. It is possible that COO^- ions and/or the imidazolyl groups may facilitate the reactions that synthesize Mg-Imidazoline and Ni-Imidazoline. We were unable to measure the pH values of the systems in this study because solid–liquid mixtures were employed. However, pH values of the liquid phases in the mixtures dropped from 7.5 (7) to 6 (5) after the hydrothermal procedure for Ni (Mg)-Imidazoline.

FT-IR absorptions assigned to COO^- were observed for the starting mixtures (Fig. 8) and crude products. Acetate ions are removed by washing with water, and this change is consistent with the change in d-value from 2.0 nm (before the wash) to 1.8 nm (after the wash) (Fig. 13).

4.3 Optical Properties

UV–Vis-NIR absorption and emission is dependent on the inorganic components. Mg-Imidazoline exhibited absorption at around 335 nm (Fig. 9a) and emission at around 410 nm

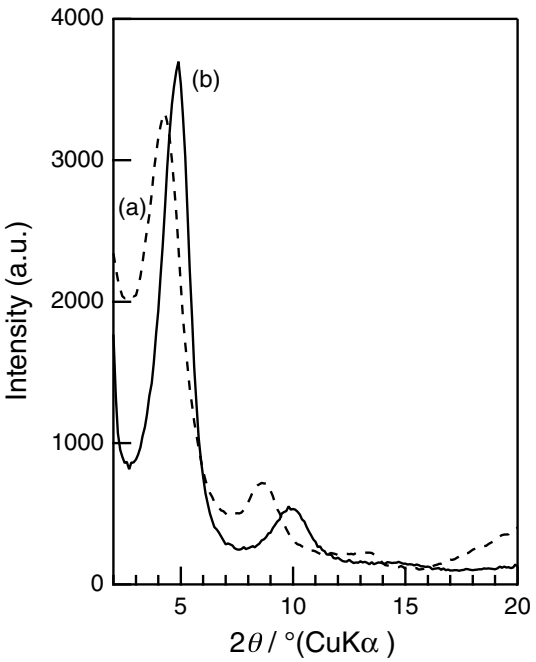

Fig. 13 XRD patterns of **a** crude product of Ni-Imidazoline and **b** Ni-Imidazoline. Pattern **a** was enlarged by a factor of 3. Pattern **b** is the same as that in Fig. 2b

(Fig. 12a), which is attributed to the imidazolyl group. In contrast we observed weak absorption due to the imidazolyl group (Fig. 9b), absorptions at around 390 nm and 680 nm (Fig. 9b), and no observable emissions (Fig. 12b) for Ni-Imidazoline, where emission was quenched by the paramagnetic Ni^{2+} (Fig. 12b). UV–Vis absorptions at around 390 nm and 680 nm (Fig. 9b) are related to oxygen coordinated nickel ions of the octahedral sheet and $[Ni(H_2O)_6]^{2+}$ [12, 38, 39], and the absorption peaks at around 390 nm (25,641 cm^{-1}) and 680 nm (14,706 cm^{-1}) are attributed to transitions $^3A_{2g} \rightarrow {}^3T_{1g}$ (P) (390 nm) and $^3A_{2g} \rightarrow {}^3T_{1g}$ (F) (680 nm) of oxygen-coordinated nickel ions in the octahedral sheet. The shoulders at the longer wavelength can be attributed to these transitions of $[Ni(H_2O)_6]^{2+}$ within the interlayer space.

The NIR spectrum showed broad absorption around 8660 cm^{-1} (1150 nm) for Ni-TEOS (Fig. 11d), which is attributed to the transition $^3A_{2g} \rightarrow {}^3T_{2g}$ of Ni (II) [38, 39]. However, NIR analysis did not indicate this absorption for Ni-Imidazoline (Fig. 11b), whereas UV–Vis analysis demonstrated absorption peaks attributed to transitions to higher energy levels than $^3T_{2g}$, i.e., $^3T_{1g}$ (Fig. 10).

The Ni octahedral sheet is sandwiched by the two imidazolylsiloxane sheets in the proposed model for Ni-Imidazoline (Scheme 2), whereas the Ni-trioctahedral sheet is sandwiched by the two Si tetrahedral sheets in Ni-TEOS, as described above. Thus, the environments around the Ni octahedral sheets are partially different in Ni-Imidazoline and Ni-TEOS. The FT-IR spectra with the sharper absorption peaks

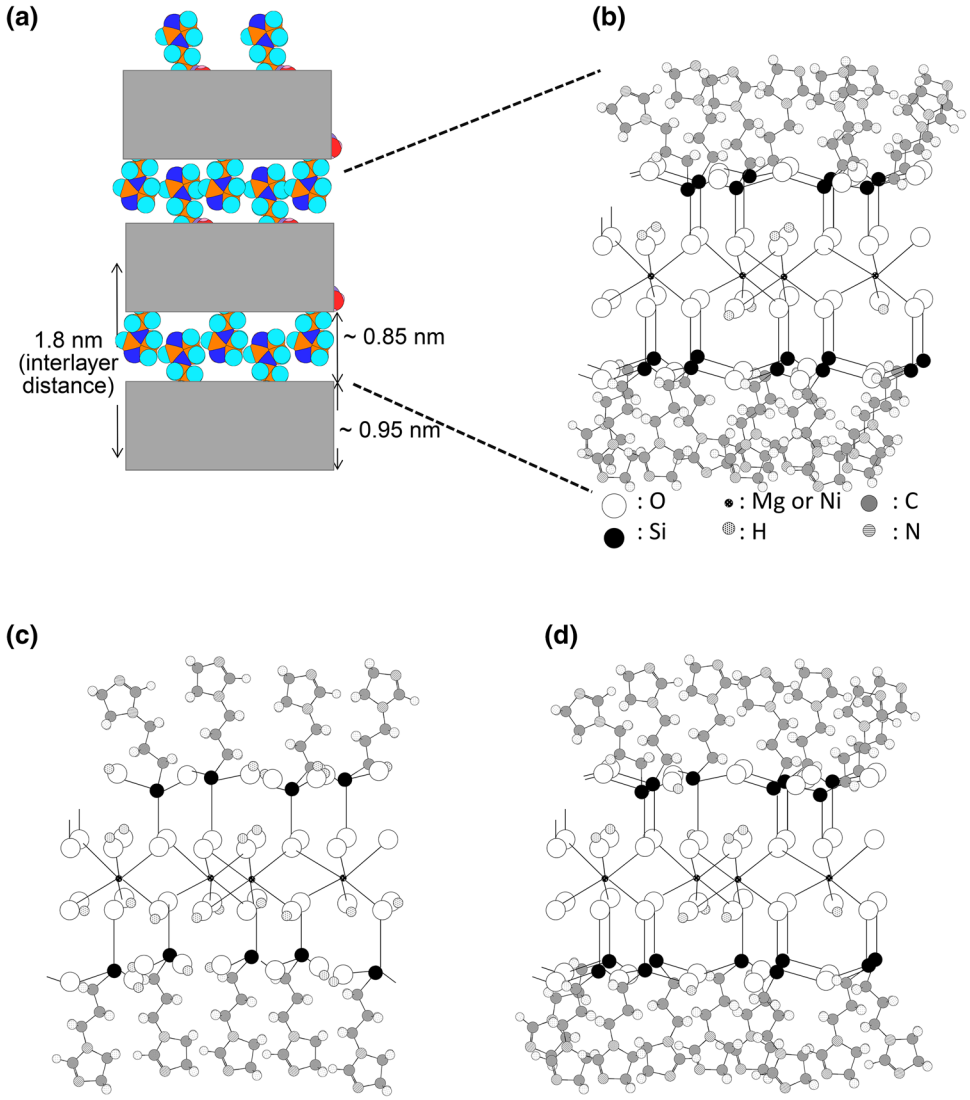

Scheme 2 Schematic representations of ***a*** proposed model for layered inorganic-imidazoline monoliths and ***b*** and ***c*** tentative and ***d*** proposed models for a layer of the monolith

for Ni-TEOS (Fig. 7d) also suggest a structure with higher regularity for the Ni-trioctahedral sheets of Ni-TEOS than for the Ni octahedral sheets of Ni-Imidazoline, as described above. We speculate that the difference in the NIR spectra between Ni-Imidazoline and Ni-TEOS (Fig. 11b, d) relates to the difference in the regularities of their structures. The low regularity of the Ni octahedral sheet splits the energy levels of Ni-Imidazoline, and absorption due to the transition becomes very broad and is not easily observed. An enlarged spectrum showed a small and broad dimple in this wavenumber region for Ni-Imidazoline (see Electronic Supplementary Material).

To summarize, Mg-Imidazoline exhibited UV–Vis absorption and emission arising from the organic moiety. In contrast, Ni-Imidazoline exhibited UV–Vis-NIR absorption related to both the inorganic and organic moieties.

5 Conclusions

We synthesized layered inorganic–imidazoline monoliths (Mg-Imidazoline and Ni-Imidazoline) from organotrialkoxysilane (ITES) and metal acetates. The analytical results enabled a model to be proposed in which the imidazolyl group is located between the 2:1 phyllosilicate-like layers and bonds covalently with them. This study also represents the first report of the optical properties of Mg-Imidazoline and Ni-Imidazoline. Mg-Imidazoline and Ni-Imidazoline exhibit properties arising from both inorganic and organic moieties, and properties due to the organic moiety are partially altered depending on the inorganic component. Ni-Imidazoline exhibits both strong absorption attributed to the inorganic moiety and weak absorption arising from the imidazolyl group, but hardly any emissions, whereas Mg-Imidazoline exhibits both absorption and emission arising from the imidazolyl group. We hope the modest results presented in this

study will help to guide future research on novel layered inorganic–organic monoliths that exhibit various functions.

Acknowledgements We are grateful to Mr. S. Takenouchi, NIMS, and Dr. A. Sato, A Rabbit Science Japan Co., Ltd., for the elemental analyses as well as Mr. K. Kosuda, NIMS, for the SEM observation. We thank Co-op Chemical Co., Ltd. (currently: Katakura & Co-op Agri Corporation) for their kind donation of the synthetic smectite sample SWN. This study was partially supported by Japan Society for the Promotion of Science (JSPS) KAKENHI (Grant Number 26420678).

References

1. V. Mittal, J. Mater. Sci. **43**, 4972 (2008)
2. A. Czímerová, N. Iyi, J. Bujdák, J. Colloid Interface Sci. **320**, 140 (2008)
3. S. Takagi, M. Eguchi, D.A. Tryk, H. Inoue, Langmuir **22**, 1406 (2006)
4. P.K. Ghosh, A.J. Bard, J. Phys. Chem. **88**, 5519 (1984)
5. N. Nhlapo, T. Motumi, E. Landman, S.M.C. Verryn, W.W. Focke, J. Mater. Sci. **43**, 1033 (2008)
6. E.P. Landman, W.W. Focke, J. Mater. Sci. **41**, 2271 (2006)
7. G.W. Brindley, G. Brown, *Crystal Structures of Clay Minerals and Their X-ray Identification* (Mineralogical Society, London, 1980)
8. F. Bergaya, G. Lagaly, *Handbook of Clay Science*, 2nd edn. (Elsevier, Amsterdam, 2013)
9. The Clay Science Society of Japan, *Nendo Handbook (Handbook of Clays and Clay Minerals)*, 3rd edn. (Gihodoshuppan, Tokyo, 2009)
10. G. Nagelschmidt, Mineral. Mag. **25**, 140 (1938)
11. G.W. Brindley, Am. Miner. **40**, 239 (1955)
12. M. Guillot, M. Richard-Plouet, S. Vilminot, J. Mater. Chem. **12**, 851 (2002)
13. N.T. Whilton, S.L. Burkett, S. Mann, J. Mater. Chem. **8**, 1927 (1998)
14. M. Richard-Plouet, S. Vilminot, M. Guillot, New J. Chem. **28**, 1073 (2004)
15. Y. Fukushima, M. Tani, Bull. Chem. Soc. Jpn. **69**, 3667 (1996)
16. Y. Fukushima, M. Tani, J. Chem. Soc. Chem. Commun. 241 (1995)
17. K.A. Carrado, L. Xu, R. Csencsits, J.V. Muntean, Chem. Mater. **13**, 3766 (2001)
18. L. Mercier, G.A. Facey, C. Detellier, J. Chem. Soc. Chem. Commun., 2111 (1994)
19. R. Ruiz-Hitzky, J.M. Rojo, Nature **287**, 28 (1980)
20. K. Chabrol, M. Gressier, N. Pebere, M.J. Menu, F. Martin, J.P. Bonino, C. Marichal, J. Brendle, J. Mater. Chem. **20**, 9695 (2010)
21. K. Fujii, S. Hayashi, H. Kodama, Chem. Mater. **15**, 1189 (2003)
22. K. Fujii, S. Hayashi, Appl. Clay Sci. **29**, 235 (2005)
23. K. Fujii, S. Hayashi, H. Hashizume, S. Shimomura, K. Jimura, T. Fujita, N. Iyi, A. Yamagishi, H. Sato, T. Ando, Phys. Chem. Chem. Phys. **18**, 19146 (2016)
24. K. Fujii, N. Iyi, R. Sasai, S. Hayashi, Chem. Mater. **20**, 2994 (2008)
25. K. Fujii, N. Iyi, H. Hashizume, S. Shimomura, T. Ando, Chem. Mater. **21**, 1179 (2009)
26. K. Fujii, T. Kuroda, K. Sakoda, N. Iyi, J. Photochem. Photobiol. A **225**, 125 (2011)
27. K. Fujii, J.P. Hill, H. Hashizume, S. Shimomura, K. Ariga, T. Ando, J. Mater. Sci. **52**, 12156 (2017)
28. Y. Turhan, P. Turhan, M. Degan, M. Alkan, H. Namli, O. Demirbas, Ind. Eng. Chem. Res. **47**, 1883 (2008)
29. K. Takahashi, J. Umeda, K. Hayashi, W. Sakamoto, T. Yogo, J. Mater. Sci. **51**, 3398 (2016)
30. R.D. Shanon, Acta Crystallogr. **A32**, 751 (1976)
31. H. Hashizume, S. Shimomura, H. Yamada, T. Fujita, H. Nakazawa, Powder Diffr. **11**, 288 (1996)
32. R.P. Teno'rio, R.P.M. Engelsberg, J.O. Fossum, G.J. da Silva, Langmuir **26**, 9703 (2010)
33. V.C. Farmer, J.D. Russel, Clays Clay Miner. **15**, 121 (1967)
34. H. Takeshi, Y. Uno, Miner. Soc. Jpn. Spec. Pap. 98 (1971)
35. Y. Uno, H. Takeshi, J. Miner. Soc. Jpn. Spec Pap. 156 (1981)
36. The Japan Society for Analytical Chemistry, *Kisobunsekikagakukoza 16 Sekigai·Raman* (Kyoritsushuppan, Tokyo, 1968)
37. J.D. Russel, V.C. Farmer, B. Velde, Mineral. Mag. **37**, 869 (1970)
38. A.F. Schreiner, D.J. Hamm, Inorg. Chem. **12**, 2037 (1973)
39. F.A. Cotton, G. Wilkinson, *Advanced Inorganic Chemistry*, 4th edn. (Wiley, New York, 1980)
40. S.W. Bailey, Clay Sci. **5**, 209 (1979)
41. M. Miyagawa, A. Shibusawa, K. Maeda, A. Tashiro, T. Sugai, H. Tanaka, RSC Adv. **7**, 41896 (2017)
42. M. Miyagawa, M. Usui, Y. Imura, S. Kuwahara, T. Sugai, H. Tanaka, Chem. Commun. **54**, 8454 (2018)
43. T. Marcopoulos, M. Economou, Am. Miner. **66**, 1020 (1981)
44. S.W. Bailey, *Hydrous Phyllosilicates* vol. 19, (Mineralogical Society of America, Washington, 1998)